

Chiral spin states in polarized kagome spin systems with spin-orbit coupling

Jia-Wei Mei,^{1,2} Evelyn Tang,² and Xiao-Gang Wen^{2,1}

¹*Institute for Advanced Study, Tsinghua University, Beijing, 100084, P. R. China*

²*Department of Physics, Massachusetts Institute of Technology, Cambridge, Massachusetts 02139, USA*
(Dated: Nov, 2010)

We study quantum spin systems with a proper combination of geometric frustration, spin-orbit coupling and ferromagnetism. We argue that such a system is likely to be in a chiral spin state, a fractional quantum Hall (FQH) state for bosonic spin degrees of freedom. The energy scale of the bosonic FQH state is of the same order as the spin-orbit coupling and ferromagnetism — overall much higher than the energy scale of FQH states in semiconductors.

I. INTRODUCTION

Landau symmetry breaking^{1,2} has been the standard theoretical concept in the classification of phases and transitions between them. However, this theory turned out insufficient when the fractional quantum Hall (FQH) state^{3,4} was discovered. These states (FQH states and spin liquids) are not distinguished by their symmetries; instead they have new topological quantum numbers such as robust ground state degeneracy^{5,6} and robust non-Abelian Berry's phases⁷. The topological order^{8,9} associated with topological quantum numbers has been proposed for the classification of these states. Recently, it was realized that topological order can be interpreted as patterns of long range quantum entanglement¹⁰⁻¹². This long range entanglement has important applications for topological quantum computation: the robust ground state degeneracy can be used as quantum memory¹³; fractional defects from the entangled states which carry fractional charges⁴ and fractional statistics¹⁴⁻¹⁶ (or non-Abelian statistics^{17,18}) can perform fault tolerant quantum computation^{19,20}.

Although it has attractive concepts and applications, topological order is only realized at very low temperatures in FQH systems^{3,4}. In this paper we present a proposal to realize highly entangled topological states at higher temperatures. The ideal is to combine geometric frustration, spin-orbit coupling and ferromagnetism in quantum spin systems. Both spin-orbit coupling and ferromagnetism can have high energy scales and appear at room temperature. Their combination breaks time-reversal symmetry which leads to rich and complicated interference from quantum spin fluctuations. In this paper we show that they can lead to highly entangled topological states at high temperatures.

Quantum spins on the kagome lattice are geometrically frustrated systems. They appear in the following compounds: Herbertsmithite $\text{ZnCu}_3(\text{OH})_6\text{Cl}_2$,²¹⁻²³ Kapellasite $\text{Cu}_3\text{Zn}(\text{OH})_6\text{Cl}_2$,²⁴ $\text{Y}_{0.5}\text{Ca}_{0.5}\text{BaCo}_4\text{O}_7$,²⁵ $\text{Mg}_x\text{Cu}_{4-x}(\text{OH})_6\text{Cl}_2$,²⁶ $\text{CaBaCo}_4\text{O}_7$,²⁷ $\text{Pr}_3\text{Ga}_5\text{SiO}_{14}$,²⁸ $\text{Nd}_3\text{Ga}_5\text{SiO}_{14}$,²⁹ $\text{BaCu}_3\text{V}_2\text{O}_8(\text{OH})_2$,³⁰ $\text{Cu}(\text{1,3-benzenedicarboxylate})$,³¹ $\text{KFe}_3(\text{OH})_6(\text{SO}_4)_2$,³² YBaCo_4O_7 ,^{33,34} $\text{YBaCo}_3\text{AlO}_7$, $\text{YBaCo}_3\text{FeO}_7$,^{33,35} $\gamma\text{-Cu}_2(\text{OD})_3\text{Cl}$,³⁶ $\text{Ni}_5(\text{TeO}_3)_4\text{Br}_2$, $\text{Ni}_5(\text{TeO}_3)_4\text{Cl}_2$,³⁷ $\text{Cu}_3\text{V}_2\text{O}_7(\text{OH})_2/2\text{H}_2\text{O}$,^{38,39}

$\text{Cs}_2\text{Cu}_3\text{CeF}_{12}$,⁴⁰ $\text{Cs}_2\text{Cu}_3\text{SnF}_{12}$, $\text{Rb}_2\text{Cu}_3\text{SnF}_{12}$,⁴¹ $\text{Cu}_2(\text{OD})_3\text{Cl}$,⁴² $\text{Cs}_2\text{Cu}_3\text{ZrF}_{12}$, $\text{Cs}_2\text{Cu}_3\text{HfF}_{12}$ ⁴³ and $\text{Co}_3\text{V}_2\text{O}_8$.⁴⁴ Motivated by these materials, in this paper we study the Heisenberg model on the kagome lattice with additional spin-orbit interaction and Zeeman coupling $\sum_i B_z S_i^z$. Some related theoretical work can be found in Ref. 45,46. In Ref. 45 a model with spin-orbit interaction but no Zeeman coupling is studied; some mean-field spin liquid states are found. In Ref. 46 a model with Zeeman coupling but no spin-orbit interaction is studied via numerical calculations. Two magnetization steps are found at $M/M_{\text{max}} = 1/3$ (stronger) and $2/3$ (weaker) for a 36 spin cluster.

In this paper, we study the state with magnetization $\langle S_i^z \rangle = 1/3$. In section II, we write down the quantum spin model with spin-orbit coupling on the Kagome lattice. In section III, we map the spin model to the hardcore bosonic model in III A, construct three trial wavefunctions for the polarized spin system $\langle S_i^z \rangle = 1/3$ in III B and then evaluate the energy expectation for these three states in III C. We find that the bosonic quantum Hall state has the lowest energy. Lastly, we discuss the materials realization in III D. In the Appendix A, we also discuss spin-orbit coupling in the transition metal oxide materials.

II. QUANTUM SPINS ON THE KAGOME LATTICE WITH SPIN-ORBIT COUPLING

The kagome lattice has 3 sites (labelled 1, 2 and 3) within every unit cell with the primitive vectors $\mathbf{a}_1 = 2a\hat{\mathbf{x}}$ and $\mathbf{a}_2 = a(\hat{\mathbf{x}} + \sqrt{3}\hat{\mathbf{y}})$ (a is the lattice constant), see Fig. 1(a). The unit cell contains one hexagon and two triangles so it is geometrically frustrated.

As shown in Fig. 1 (b), the triangle Δ_{123} on the kagome plane in Herbertsmithite $\text{ZnCu}_3(\text{OH})_6\text{Cl}_2$ ²¹⁻²³ contains three copper cations surrounded by distorted octahedrons sharing one chlorine corner while each pair shares an oxygen corner. Mediated by this oxygen, the $\text{Cu } 3d^9$ electron hops from site \mathbf{r}_1 to \mathbf{r}_2 , e.g. see Fig. 1(c).

Inversion symmetry for Herbertsmithite breaks down explicitly, leading to a non-uniform charge distribution in the kagome lattice. For convenience, we model the charge

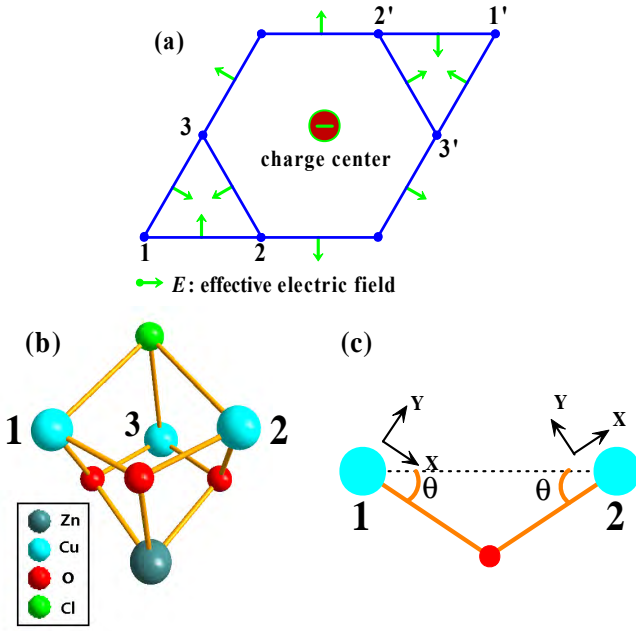


FIG. 1: (color online) (a) The kagome lattice with three different sites $l = 1, 2, 3$ within the unit cell. Inversion symmetry breaking via a charge center in the hexagon leads to the effective electric field \mathbf{E}_{ij} on the bond \mathbf{r}_{ij} , represented by green arrows which point from the middle of the bond to the center of every triangle on the kagome lattice. (b) The triangle Δ_{123} in the kagome lattice for Herbertsmithite^{21–23}. (c) The nearest neighbor bond \mathbf{r}_{12} : the electron hops from site \mathbf{r}_1 to \mathbf{r}_2 mediated by the oxygen atom.

center as being in the hexagon, see Fig.1(a). When hopping from \mathbf{r}_1 to \mathbf{r}_2 , the electron sees the electric field \mathbf{E}_{12} (labelled by the green arrow in Fig. 1(a)). The effective electric field couples to the electron through the spin-orbit coupling vector $\mathbf{D}_{12} = \alpha \mathbf{E}_{12} \times \mathbf{r}_{12}$ in the Rashba manner, where $\mathbf{r}_{12} = \mathbf{r}_1 - \mathbf{r}_2$ ⁴⁷

$$t_{12} = -t \sum_{\sigma\sigma'} \left(\exp(-i\vec{\sigma} \cdot \mathbf{D}_{12})_{\sigma\sigma'} c_{1\sigma}^\dagger c_{2\sigma'} + \text{h.c.} \right) \quad (1)$$

Here $\vec{\sigma} = (\sigma_x, \sigma_y, \sigma_z)$ are the Pauli matrices. The coefficient α should be chosen to make the spin-orbit coupling vector \mathbf{D}_{12} dimensionless. Note that $\mathbf{D}_{12} = -\mathbf{D}_{21}$.

Including on-site interactions we obtain the Hubbard model with spin-orbit coupling for $S = 1/2$ electrons on the kagome lattice

$$H = -t \sum_{\sigma\sigma'} \left((e^{-i\vec{\sigma} \cdot \mathbf{D}_{ij}})_{\sigma\sigma'} c_{i\sigma}^\dagger c_{j\sigma'} + \text{h.c.} \right) + U \sum_i n_{i\uparrow} n_{i\downarrow} \quad (2)$$

where i and j denote nearest neighbors.

For a specified bond \mathbf{r}_{ij} , we can make a gauge transformation⁴⁸

$$\begin{aligned} c_{i\sigma} &\rightarrow \tilde{c}_{i\sigma} = \sum_{\sigma'} (e^{i(D/2)\vec{\sigma} \cdot \mathbf{n}_{ij}})_{\sigma\sigma'} c_{i\sigma'} \\ c_{j\sigma} &\rightarrow \tilde{c}_{j\sigma} = \sum_{\sigma'} (e^{-i(D/2)\vec{\sigma} \cdot \mathbf{n}_{ij}})_{\sigma\sigma'} c_{j\sigma'} \end{aligned} \quad (3)$$

where $\mathbf{D}_{ij} = \mathbf{n}_{ij} D$. Then

$$H = -t \sum_{\sigma} (\tilde{c}_{i\sigma}^\dagger \tilde{c}_{j\sigma} + \text{h.c.}) + U \sum_i \tilde{n}_{i\uparrow} \tilde{n}_{i\downarrow} \quad (4)$$

Using standard second-order perturbation theory, we obtain the exchange term

$$J_{ij} = J \tilde{\mathbf{S}}_i \cdot \tilde{\mathbf{S}}_j \quad (5)$$

Here $J = 4t^2/U$ is the exchange coupling for the rotated spin operator $\tilde{\mathbf{S}}_i = \sum_{\sigma\sigma'} \tilde{c}_{i\sigma} \vec{\sigma}_{\sigma\sigma'} \tilde{c}_{j\sigma'}$.

On the kagome lattice, we cannot find a gauge transformation as in Eq. (3) that would be compatible for each site. So we have to write the Hamiltonian in terms of the original spin operators. On every bond, the rotated spin operators are related to the original ones as follows:

$$\begin{aligned} \tilde{S}_i &= (1 - \cos(D))(\hat{\mathbf{n}}_{ij} \cdot \mathbf{S}_i) \hat{\mathbf{n}}_{ij} + \cos(D) \mathbf{S}_i \\ &\quad - \sin(D) \mathbf{S}_i \times \hat{\mathbf{n}}_{ij} \end{aligned} \quad (6)$$

$$\begin{aligned} \tilde{S}_j &= (1 - \cos(D))(\hat{\mathbf{n}}_{ij} \cdot \mathbf{S}_j) \hat{\mathbf{n}}_{ij} + \cos(D) \mathbf{S}_j \\ &\quad + \sin(D) \mathbf{S}_j \times \hat{\mathbf{n}}_{ij} \end{aligned} \quad (7)$$

Thus we obtain the quantum spin model on the kagome lattice including spin-orbit coupling⁴⁸

$$\begin{aligned} H &= J \sum_{\langle ij \rangle} (\cos(2D) \mathbf{S}_i \cdot \mathbf{S}_j + \sin(2D) (\mathbf{S}_i \times \mathbf{S}_j) \cdot \hat{\mathbf{n}}_{ij} \\ &\quad + 2 \sin^2(D) (\mathbf{S}_i \cdot \hat{\mathbf{n}}_{ij}) (\mathbf{S}_j \cdot \hat{\mathbf{n}}_{ij})) \end{aligned} \quad (8)$$

III. POLARIZED SPIN STATE WITH TOPOLOGICAL ORDER

A. Hardcore bosonic model

For simplicity we choose the spin-orbit coupling vectors \mathbf{D}_{ij} perpendicular to the kagome plane: $\mathbf{D}_{12} = \mathbf{D}_{23} = \mathbf{D}_{31} = \mathbf{D}_{1'2'} = \mathbf{D}_{2'3'} = \mathbf{D}_{3'1'} = D \hat{\mathbf{z}}$ (only in-plane effective electric fields \mathbf{E}_{ij} are considered). We use the Holstein-Primakoff transformation:

$$S_i^+ = b_i^\dagger, \quad S_i^- = b_i, \quad S_i^z = \frac{1}{2} - b_i^\dagger b_i \quad (9)$$

where b_i is the hardcore bosonic operator $[b_i, b_j^\dagger] = \delta_{ij}$, $n_i = b_i^\dagger b_i \leq 1$. This maps the spin model (8) onto a hardcore bosonic model^{49,50}

$$\begin{aligned} H &= \frac{J}{2} \sum_{\langle ij \rangle} \left(\exp[i(\hat{\mathbf{n}}_{ij} \cdot \hat{\mathbf{z}}) 2D] b_i^\dagger b_j + \text{h.c.} \right) \\ &\quad + J \sum_{\langle ij \rangle} n_i n_j \end{aligned} \quad (10)$$

which describes interacting hardcore systems with hopping under effective fluxes as shown in Fig. 2: within the triangles Δ_{123} and $\nabla_{1'2'3'}$, there are fluxes $\phi_1 = 6D$; in

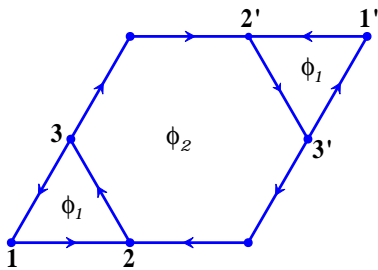


FIG. 2: (color online) Flux distribution for the hardcore bosons.

the hexagon, there is flux $\phi_2 = -2\phi_1$. When $\phi_1 \neq 0, \pi \text{ mod } 2\pi$, these effective fluxes break time-reversal symmetry for this model.

Now let us consider just one boson described by only the hopping term in the above Hamiltonian. The hopping Hamiltonian has three bands. We calculate the Berry curvatures over the Brillouin zone for the lowest band in the presence of the flux for different spin-orbit couplings: $D = 0.025, 0.1$ and $\pi/8$. The Berry curvature is defined as follows

$$F_n(\mathbf{k}) = \epsilon_{ij} \partial_{k_i} A_j^{(n)}(\mathbf{k}), \quad A_i^{(n)}(\mathbf{k}) = i \langle u_{n\mathbf{k}} | \partial_{k_i} | u_{n\mathbf{k}} \rangle \quad (11)$$

where $u_{n\mathbf{k}}$ is the Bloch wave packet in the n -th band of the hopping Hamiltonian

$$H_t = \frac{J}{2} \sum_{\langle ij \rangle} \left(\exp[i(\hat{\mathbf{n}}_{ij} \cdot \hat{\mathbf{z}})i2D] b_i^\dagger b_j + \text{h.c.} \right) \quad (12)$$

$$H_t |u_{n\mathbf{k}}\rangle = \epsilon_{n\mathbf{k}} |u_{n\mathbf{k}}\rangle$$

In this paper, instead of using \hat{k}_x and \hat{k}_y as the axes in k -space, we use $\hat{k}_1 = k_x$ and $\hat{k}_2 = (k_x + \sqrt{3}\hat{k}_y)/2$ for convenience. The dispersion $\epsilon_{n\mathbf{k}}$ has three bands (labelled $n = b$ for the bottom band, $n = m$ for the middle band and $n = t$ for the top band) as shown in Fig. 3 (a), (c) and (e). In all cases ($D = 0.025, D = 0.1$ and $D = \pi/8$) the three bands have nonzero Chern numbers $C_b = 1, C_m = 0$ and $C_t = -1$, where the Chern number $C \equiv \frac{1}{2\pi} \int_{\text{BZ}} d^2k F_n(\mathbf{k})$.

We plot the Berry curvature of the bottom band for $D = 0.025, 0.1$ and $\pi/8$ in Fig. 3 (b), (d) and (f). We see that when $D = 0.1$, the lowest band is separated from the other bands by an energy gap and the lowest band is quite flat. Since the lowest band has a non-zero Chern number $C_b = 1$, it simulates the first Landau level in free space. By analogy to the quantum Hall effect in high magnetic field, the hardcore bosons are likely to form a $\nu = 1/2$ bosonic quantum Hall state when there is half a boson per unit cell. The boson filling number is $f = 1/6$ per site which corresponds to the spin polarization

$$\langle S_i^z \rangle = 1/2 - f = 1/3 \quad (13)$$

In other words, the polarized spin state $\langle S_i^z \rangle = 1/3$ is likely to be a chiral spin liquid⁵¹ — a topologically ordered state.

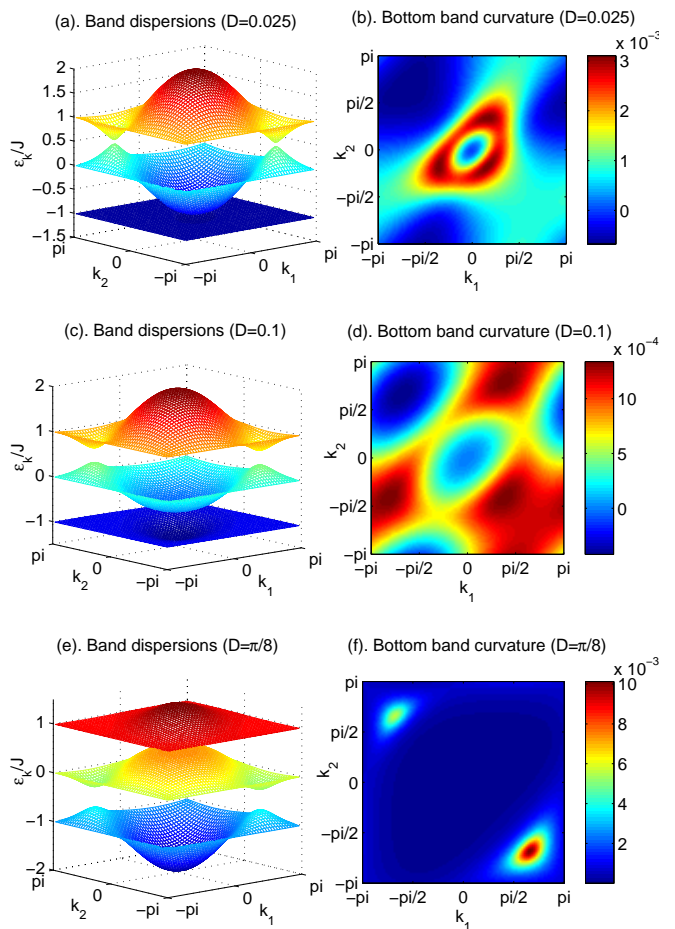


FIG. 3: (color online) (a), (c) and (e): Band dispersions of the hardcore boson in the presence of the flux as shown in Fig. 2 for $D = 0.025, D = 0.1$ and $D = \pi/8$, respectively; (b), (d) and (f) are the corresponding bottom band curvatures for (a), (c) and (e).

B. Fermionic constructions for the bosonic wavefunctions

To study the topologically ordered chiral spin state, we will employ the fermionic approach to construct trial bosonic wavefunctions. The many-body bosonic wavefunction can be represented as follows

$$|\Phi\rangle = \sum_{\{x_1, \dots, x_{N_b}\}} \Phi(x_1, \dots, x_{N_b}) |\{x_i\}\rangle \quad (14)$$

Here the sum is over all possible boson configurations $|\{x_i\}\rangle = |\{x_1, \dots, x_{N_b}\}\rangle = a_{x_1}^\dagger \dots a_{x_{N_b}}^\dagger |0\rangle$ and $\Phi(x_1, \dots, x_{N_b})$ is the symmetric wavefunction. In this paper, we are only concerned with translationally invariant ground states.

The many-body bosonic wave function for a product

state (PS) has the form

$$\Phi(x_1, \dots, x_{N_b}) = \prod_{i=1}^N \phi_l(x_i) \quad (15)$$

where $\phi_l(x_i + \mathbf{a}_j) = \phi_l(x_i)$ to maintain translational invariance. $l = 1, 2, 3$ denotes sites within the unit cell and the vector \mathbf{a}_j , $j = 1, 2$, is a Bravais vector for the kagome lattice. So the many-body wave function is labelled by three complex parameters ϕ_1 , ϕ_2 , and ϕ_3 corresponding to the spin orientation on the three sites in each unit cell. The mean field ground state of this type is obtained by minimizing the average energy by varying ϕ_1 , ϕ_2 , and ϕ_3 . This type of spin ordered states without topological order is the main competing state for the ground state of our model.

To construct the bosonic ground state with topological order, we split the the hardcore boson into two species of fermions

$$b_i = \alpha_i \beta_i \quad (16)$$

where α_i and β_i are fermion operators which satisfy the constraint on every site: $n_{i\alpha} = n_{i\beta} = n_{ib}$. The configuration becomes

$$|\{x_i\}\rangle = \alpha_{x_1}^\dagger \beta_{x_1}^\dagger \dots \alpha_{x_{N_b}}^\dagger \beta_{x_{N_b}}^\dagger |0\rangle \quad (17)$$

and the symmetric wave function factorizes as follows

$$\Phi(\{x_i\}) = \Psi_\alpha(\{x_i\}) \Psi_\beta(\{x_i\}) \quad (18)$$

where $\Psi_\alpha(\{x_i\})$ and $\Psi_\beta(\{x_i\})$ are the antisymmetric fermionic wavefunctions for α_i and β_i . Using this fractionalization we construct two ansatz wavefunctions: the bosonic quantum Hall state (QHS) and the spin Hall state (SHS).

The fermionic wavefunctions $\Psi_\alpha(\{x_i\})$ and $\Psi_\beta(\{x_i\})$ can be constructed from the mean field tight binding Hamiltonian

$$\begin{aligned} H_\alpha &= -t_{\text{eff}} \sum_{\langle ij \rangle} \left(\alpha_i^\dagger \alpha_j \exp(iA_{ij}^\alpha) + \text{h.c.} \right) \\ H_\beta &= -t_{\text{eff}} \sum_{\langle ij \rangle} \left(\beta_i^\dagger \beta_j \exp(iA_{ij}^\beta) + \text{h.c.} \right) \end{aligned} \quad (19)$$

The filling factors for the fermions α_i, β_i are $f = 1/6$ per site, namely half per unit cell. For the QHS and SHS, we need the filling factor corresponding to one particle per unit cell which can be realized by inserting half a flux quantum ($\phi = \pi$) in the original unit cell to double the unit cell:

$$\phi_2^\omega + 2\phi_1^\omega = \pi, \quad \omega = \alpha, \beta \quad (20)$$

where ϕ_1^ω and ϕ_2^ω are fluxes in the kagome unit cell, see Fig. 2. In the presence of these fluxes, we specify a gauge for A_{ij}^ω in this tight-binding model (19) to obtain single particle wavefunctions in the bottom band: $\psi_\omega(\mathbf{k}_i, x_j)$

($\omega = \alpha, \beta$), where \mathbf{k} is the Bloch momentum vector for the doubled unit cell. Thus the fermionic wavefunctions are the determinants of these single particle wave functions:

$$\Psi_\omega(\{x_i\}) = \det[\psi_\omega(\mathbf{k}_i, x_j)] \quad (21)$$

where $\omega = \alpha, \beta$ and $i, j = 1, 2, \dots, N_b$. For the QHS state, we set $\phi_1^\alpha = \phi_1^\beta$ and $\phi_2^\alpha = \phi_2^\beta$; for the SHS state, we set $\phi_1^\alpha = -\phi_1^\beta$ and $\phi_2^\alpha = -\phi_2^\beta$. For the QHS, each fermion has the same Chern number $C_\omega = 1$; for the SHS, $C_\alpha = 1$ and $C_\beta = -1$.

We now consider the effective theory for the QHS and SHS. For the QHS and SHS, fermionic excitations are gapped out. There is a gauge freedom for the fractionalization in Eq. (16): the gauge transformation $\alpha_i \rightarrow \alpha_i e^{i\theta_i}$, $\beta_i \rightarrow \beta_i e^{-i\theta_i}$ does not change the bosonic operator b_i . The Hamiltonian with the gauge fluctuations is given by

$$\begin{aligned} H_\alpha &= -t_{\text{eff}} \sum_{\langle ij \rangle} \left(\alpha_i^\dagger \alpha_j \exp(i\tilde{A}_{ij} + ia_{ij}) + \text{h.c.} \right) \\ H_\beta &= -t_{\text{eff}} \sum_{\langle ij \rangle} \left(\beta_i^\dagger \beta_j \exp(-i\tilde{A}_{ij} - ia_{ij}) + \text{h.c.} \right) \end{aligned} \quad (22)$$

The non-zero Chern number for each fermion species implies that the low energy effective action for the gauge fields is given by

$$\mathcal{L} = \frac{i}{4\pi} \sum_\omega C_\omega \epsilon_{\mu\nu\lambda} a_\mu \partial_\nu a_\lambda + \dots \quad (23)$$

where ... represents higher order terms. For the QHS, $C_\alpha = C_\beta = 1$ so we obtain the low-energy effective theory

$$\mathcal{L}_{\text{QHS}} = \frac{i}{2\pi} \epsilon_{\mu\nu\lambda} a_\mu \partial_\nu a_\lambda + \frac{1}{4\pi^2 g} (\epsilon_{\mu\nu\lambda} \partial_\nu a_\lambda)^2 \quad (24)$$

This describes the $\nu = 1/2$ FQH state for bosons corresponding to the chiral spin state first introduced in Ref. 51. We note that although the α and β fermions have the same Chern number, the sign of the coupling of each fermion to the $U(1)$ gauge field a_μ is opposite. Thus a 2π flux of a_μ creates an α fermion and annihilates a β fermion.

For the SHS, $C_\alpha = 1$, $C_\beta = -1$ and we obtain the low-energy effective theory

$$\mathcal{L}_{\text{SHS}} = \frac{1}{4\pi^2 g} (\epsilon_{\mu\nu\lambda} \partial_\nu a_\lambda)^2 \quad (25)$$

Here the α and β fermions in the SHS have opposite Chern number and the sign of the coupling of the two fermions to the $U(1)$ gauge field a_μ is also opposite. Thus a 2π flux of a_μ creates an α fermion and a β fermion which corresponds to a b boson, i.e. it describes a spin flip. So the magnetic field of the $U(1)$ gauge field a_μ corresponds to the spin S^z density. Since spin S^z is conserved, the $U(1)$ instanton is forbidden. Thus the 2+1D $U(1)$ gauge

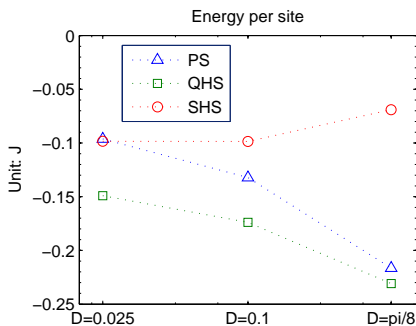


FIG. 4: (color online) Energy per site for $D = 0.025$, $D = 0.1$ and $D = \pi/8$ respectively.

theory above is not confined and the $U(1)$ gauge field a_μ remains gapless. As this gapless $U(1)$ gauge field corresponds to the spin S^z density, the gapless spin density fluctuations imply that $e^{i\theta S^z}$ spin rotation is spontaneously broken. Thus the SHS is a spin XY ordered state.

C. Numerical results

For the three different states (PS, QHS and SHS), we can evaluate the expected energies for the bosonic model (10):

$$E(\Phi) = \frac{\langle \Phi | H | \Phi \rangle}{\langle \Phi | \Phi \rangle} = \sum_{\{x_i\}} e_L(\{x_i\}) \frac{|\langle \{x_i\} | \Phi \rangle|^2}{\langle \Phi | \Phi \rangle} \quad (26)$$

where we define the local energy $e_L(\{x_i\}) = \frac{\langle \Phi | H | \{x_i\} \rangle}{\langle \Phi | \{x_i\} \rangle}$. We evaluate the energy in (26) by appropriately averaging the local energy $e_L(\{x_i\})$ over a set of configurations $|\{x_i\}\rangle$ distributed according to the square of the wave function $|\langle \{x_i\} | \Phi \rangle|^2$, generated with a standard variational Monte Carlo method.

Then we use a minimization function to optimize the expectation values on an 8×8 lattice. In Fig. 4, we plot the energy per site of the three states for $D = 0.025$, $D = 0.1$ and $D = \pi/8$. For $D = 0.025$, the PS and SHS have energies close to each other. The QHS has a better energy. As the spin-orbit coupling is increased, the SHS becomes worse in energy. Both the PS and QHS gain in energy and the PS gains much more. When $D = \pi/8$, the PS gives results close to the QHS. With small spin-orbit coupling ($D = 0.025$ and $D = 0.1$), the bottom band of the hopping Hamiltonian in (10) is flat and has a smooth curvature over the Brillouin zone. The classic PS cannot gain much energy through condensation of the lowest states. When D increases, the bottom band becomes more convex and the PS will gain a lot of energy through condensation.

Our numerical results indicate that the topologically ordered QHS (the chiral spin state) is a serious candidate for a kagome spin system with spin-orbit coupling and

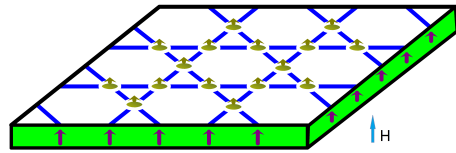


FIG. 5: (color online) A scheme to tune the filling number of hardcore bosons b_i : the kagome lattice couples to a ferromagnetic substrate by the exchange interaction $H_{\text{int}} = J_{\text{ex}} \sum_i \mathbf{S}_i^m \cdot \mathbf{S}_i$; we can tune the substrate magnetization $\langle \mathbf{S}_i^m \rangle$ by an applied magnetic field.

spin polarization. This may be a realistic route for the discovery of new topologically ordered states in quantum spin systems.

D. Practical realization

Here we explore the possibility of obtaining a polarized state ($S_i^z \neq 0$) experimentally. This can be achieved by applying a magnetic field, which adds a term $H_h = -B \sum_i n_i$ to the Hamiltonian (10). However, the exchange energy $J \sim 100\text{meV}$ is usually very large, so experimentally accessible magnetic fields cannot polarize the spin to $S^z = 1/3$. Hence we should find other ways of obtaining a large effective magnetic field.

One way is to place the kagome lattice on a ferromagnetic substrate, see Fig. 5. The exchange interaction is $H_{\text{int}} = J_{\text{ex}} \sum_i \mathbf{S}_i^m \cdot \mathbf{S}_i$, here J_{ex} is the exchange coupling between spins \mathbf{S}_i^m on the substrate and spins \mathbf{S}_i on the kagome plane. The exchange coupling J_{eff} can be very large when the kagome plane structure matches that of the substrate perfectly. Such a large effective magnetic field can polarize the spin on the kagome lattice.

A third way is to insert ferromagnetic atoms in the kagome system. If these ferromagnetic atoms form a ferromagnetic state, the exchange interaction can also induce spin polarization on the kagome lattice.

IV. SUMMARY

In this paper, we study quantum spin systems on the kagome lattice with spin-orbit coupling and spin polarization. We argue that such a system can be in a topologically ordered chiral spin state, a FQH state for bosonic spin degrees of freedom. The energy scale of the bosonic FQH state is of the same order as the spin-orbit coupling and ferromagnetism — overall much higher than the energy scale of FQH states in semiconductors. This result suggests exploration of topologically ordered states in quantum spin systems with a proper combination of geometric frustration, spin-orbital coupling and ferromagnetism.

This research is supported by NSF Grant No. DMR-1005541 and NSFC 11074140.

Appendix A: Discussion of spin-orbit coupling

The Rashba spin-orbit coupling is weak, around $|D| = 0.025$ for Herbertsmithite $\text{Zn Cu}_3(\text{OH})_6\text{Cl}_2$. This small value prompts us to find other mechanisms to increase the strength of the spin-orbit coupling.

In the literature, the spin-orbit coupling is also discussed on the atomic level and with a large strength of coupling, e.g. around 0.2 eV and 0.4 eV for the 4d and 5d electrons, respectively. We hope to relate the atomic spin-orbit coupling to the form represented in Eq. 1. This has been achieved for the $5d^5$ electron in Sr_2IrO_4 ⁵² and we discuss the general case below.

A $S = 1/2$ electron can be found in d^1 , d^5 and d^9 orbitals in transition metal cations, e.g. in Mo^{5+} , Ir^{4+} and Cu^{2+} respectively. Due to the crystal field, the fivefold degenerate d state is split into a doublet e_g and a triplet t_{2g} . d^1 and d^5 with a ligand octahedron and d^9 with a ligand tetrahedron belong to t_{2g} . The triplet t_{2g} has strong spin-orbit coupling

$$H_i = \lambda \mathbf{l}_i \cdot \mathbf{s}_i. \quad (\text{A1})$$

Here \mathbf{s}_i is the spin operator and $l = 1$ is the effective angular momentum with $|l_z^z = 0\rangle \equiv |XY\rangle_i$ and $|l_z^z = \pm 1\rangle \equiv -\frac{1}{\sqrt{2}}(i|XZ\rangle_i \pm |YZ\rangle_i)$ (X , Y and Z are local axes supporting by the local octahedron or tetrahedron, e.g. see Fig. 1(b)). The strong spin-orbit coupling (A1) splits t_{2g} into two groups with effective angular momentum $J_{\text{eff}}^z = 1/2$ and $J_{\text{eff}}^z = 3/2$, respectively. The $J_{\text{eff}}^z = 1/2$ singlet contains a Kramers doublet: $|\tilde{\uparrow}\rangle_i = \frac{\sqrt{2}}{3}|-1, \uparrow\rangle_i + \frac{1}{3}|0, \downarrow\rangle_i$ and $|\tilde{\downarrow}\rangle_i = \frac{\sqrt{2}}{3}|+1, \downarrow\rangle_i + \frac{1}{3}|0, \uparrow\rangle_i$. Here we are concerned with the Kramers doublet labelled by the pseudospin $\tilde{\mathbf{s}}_i = \tilde{\sigma}_i/2$.

There is a p bond between the cation and mediating oxygen atom. When the two cations and oxygen lie on a straight line along the bond, the values of the overlap for $\langle l_z = 0|p\rangle_{\text{O}}$ and $\langle l_z = \pm 1|p\rangle_{\text{O}}$ are the same. In Herbertsmithite, they are not along a straight line and form a triangle, see Fig. 1(c). As a result, different orbits have different overlaps with the p orbital in the oxygen $\langle \tilde{\sigma}|p\rangle_{\text{O}}$

when the electron hops on the bond \mathbf{r}_{12} from \mathbf{r}_1 to \mathbf{r}_2 :

$$|\langle l_z = \pm 1|p\rangle_{\text{O}}| > |\langle l_z = 0|p\rangle_{\text{O}}| \quad (\text{A2})$$

For the sake of simplicity, we neglect the overlap $|\langle l_z = 0|p\rangle_{\text{O}}|$ here and are only concerned with $|\langle l_z = \pm 1|p\rangle_{\text{O}}|$. Then we can write the spin-orbit in terms of the pseudospin in this manner

$$H_i \sim \lambda \mathbf{l}(\mathbf{r}_i) \cdot \tilde{\mathbf{s}}(\mathbf{r}_i) \quad (\text{A3})$$

Here the orbital angular momentum $\mathbf{l}(\mathbf{r}_i)$ can be regarded as the effective magnetic field on the pseudospin $\tilde{\mathbf{s}}(\mathbf{r}_i)$. It is very interesting that the orientation of the *magnetic field* $\mathbf{l}(\mathbf{r}_i)$ varies from each site \mathbf{r}_i . When the hopping encloses a loop, e.g. Δ_{123} in Fig. 1 (b), an electron obtains a non-zero Berry phase ϕ_{Berry} related to the spin-orbit coupling vector \mathbf{D} in Eq. (1) as follows

$$\phi_{\text{Berry}} = \oint_{\Omega} d\mathbf{r} \cdot \mathbf{D}(\mathbf{r}) \quad (\text{A4})$$

where Ω is the closed loop.

To rotate the Kramers doublet from the local axes (X , Y and Z) to the global axes (x , y and z) we use

$$|\tilde{\sigma}; \{x\}\rangle = (e^{i\tilde{\sigma} \cdot \mathbf{n}_i \theta/2})_{\alpha\sigma} |\alpha; \{X\}\rangle \quad (\text{A5})$$

where $\{x\} = e^{i\mathbf{l}_i \cdot \mathbf{n}_i \theta} \{X\}$. The hopping process on the bond \mathbf{r}_{12} is given as

$$t_{12} = \sum_{\sigma\sigma'} \left(t_{\sigma\sigma'}(\mathbf{r}_1, \mathbf{r}_2) c_{1\sigma}^\dagger c_{2\sigma'} + \text{h.c.} \right) \quad (\text{A6})$$

with the hopping parameter

$$\begin{aligned} t_{\sigma\sigma'}(\mathbf{r}_1, \mathbf{r}_2) &\sim (e^{-i\tilde{\sigma} \cdot \mathbf{n}_{12} \theta})_{\sigma\sigma'} \langle \pm 1 | O_p \rangle \langle O_p | \pm 1 \rangle_2 \\ &\equiv -t(e^{-i\tilde{\sigma} \cdot \mathbf{n}_{12} \theta})_{\sigma\sigma'} \end{aligned} \quad (\text{A7})$$

This is exactly the same as in Eq. (1) when $\mathbf{D}_{12} = \mathbf{n}_{12}\theta$. The Berry phase can be very large on the Kagome lattice resulting a very strong spin-orbit coupling effect.

¹ L. D. Landau, Phys. Z. Sowjetunion **11**, 26 (1937).
² L. D. Landau and E. M. Lifschitz, *Statistical Physics - Course of Theoretical Physics Vol 5* (Pergamon, London, 1958).
³ D. C. Tsui, H. L. Stormer, and A. C. Gossard, Phys. Rev. Lett. **48**, 1559 (1982).
⁴ R. B. Laughlin, Phys. Rev. Lett. **50**, 1395 (1983).
⁵ X.-G. Wen, Phys. Rev. B **40**, 7387 (1989).
⁶ X.-G. Wen and Q. Niu, Phys. Rev. B **41**, 9377 (1990).
⁷ F. Wilczek and A. Zee, Phys. Rev. Lett. **52**, 2111 (1984).
⁸ X.-G. Wen, Int. J. Mod. Phys. B **4**, 239 (1990).
⁹ X.-G. Wen, Advances in Physics **44**, 405 (1995).
¹⁰ A. Kitaev and J. Preskill, Phys. Rev. Lett. **96**, 110404 (2006).

¹¹ M. Levin and X.-G. Wen, Phys. Rev. Lett. **96**, 110405 (2006).
¹² X. Chen, Z.-C. Gu, and X.-G. Wen(2010), arXiv:1004.3835.
¹³ E. Dennis, A. Kitaev, A. Landahl, and J. Preskill, J. Math. Phys. **43**, 4452 (2002).
¹⁴ J. M. Leinaas and J. Myrheim, Il Nuovo Cimento **37B**, 1 (1977).
¹⁵ F. Wilczek, Phys. Rev. Lett. **49**, 957 (1982).
¹⁶ D. Arovas, J. R. Schrieffer, and F. Wilczek, Phys. Rev. Lett. **53**, 722 (1984).
¹⁷ G. Moore and N. Read, Nucl. Phys. B **360**, 362 (1991).
¹⁸ X.-G. Wen, Phys. Rev. Lett. **66**, 802 (1991).
¹⁹ A. Y. Kitaev, Ann. Phys. (N.Y.) **303**, 2 (2003).

- ²⁰ C. Nayak, S. H. Simon, A. Stern, M. Freedman, and S. D. Sarma, *Rev. Mod. Phys.* **80**, 1083 (2008), arXiv:0707.1889.
- ²¹ J. S. Helton, K. Matan, M. P. Shores, E. A. Nytko, B. M. Bartlett, Y. Yoshida, Y. Takano, A. Suslov, Y. Qiu, J.-H. Chung, D. G. Nocera, and Y. S. Lee, *Phys. Rev. Lett.* **98**, 107204 (2007), arXiv:cond-mat/0610539.
- ²² I. Rousochatzakis, S. R. Manmana, A. M. Läuchli, B. Normand, and F. Mila, *Phys. Rev. B* **79**, 214415 (2009), arXiv:0903.2884.
- ²³ Z. Hiroi, H. Yoshida, Y. Okamoto, and M. Takigawa, *J. Phys.: Conf. Ser.* **145**, 012002 (2009), arXiv:0810.4202.
- ²⁴ R. H. Colman, C. Ritter, and A. S. Wills, *Chem. Mater.* **20**, 6897 (2008), arXiv:0811.4048.
- ²⁵ J. R. Stewart, G. Ehlers, H. Mutka, C. Payen, P. Fouquet, and R. Lortz(2010), arXiv:1005.1883.
- ²⁶ S. Chu, T. M. McQueen, R. Chisnell, D. E. Freedman, P. Müller, Y. S. Lee, and D. G. Nocera, *J. Am. Chem. Soc.* **132**, 5570 (2010), arXiv:1004.0941.
- ²⁷ V. Caignaert, V. Pralong, V. Hardy, C. Ritter, and B. Raveau(2010), arXiv:1002.4544.
- ²⁸ A. Zorko, F. Bert, P. Mendels, K. Marty, and P. Bordet, *Phys. Rev. Lett.* **104**, 057202 (2010), arXiv:0912.4648.
- ²⁹ J. Robert, V. Simonet, B. Canals, R. Ballou, P. Bordet, P. Lejay, and A. Stunault, *Phys. Rev. Lett.* **96**, 197205 (2006), arXiv:cond-mat/0602457.
- ³⁰ W.-M. Zhang, H. Ohta, S. Okubo, M. Fujisawa, T. Sakurai, Y. Okamoto, H. Yoshida, and Z. Hiroi(2009), arXiv:0912.4335.
- ³¹ L. Marcipar, O. Ofer, A. Keren, E. A. Nytko, D. G. Nocera, Y. S. Lee, J. S. Helton, and C. Baines(2009), arXiv:0909.4187.
- ³² K. Matan, J. S. Helton, D. Grohol, D. G. Nocera, S. Wakimoto, K. Kakurai, and Y. S. Lee, *Physica B* **404**, 2529 (2009), arXiv:0908.2670.
- ³³ D. D. Khalyavin, P. Manuel, B. Ouladdiaf, A. Huq, H. Zheng, J. F. Mitchell, and L. C. Chapon(2010), arXiv:1007.4683.
- ³⁴ D. D. Khalyavin, P. Manuel, J. F. Mitchell, and L. C. Chapon(2010), arXiv:1008.0766.
- ³⁵ N. Hollmann, Z. Hu, M. Valldor, A. Maignan, A. Tanaka, H. H. Hsieh, H.-J. Lin, C. T. Chen, and L. H. Tjeng, *Phys. Rev. B* **80**, 085111 (2009), arXiv:0908.0226.
- ³⁶ A. S. Wills, T. G. Perring, S. Raymond, B. Fak, J.-Y. Henry, and M. Telling, *J. Phys.: Conf. Ser.* **145**, 012056 (2009), arXiv:0907.1230.
- ³⁷ J. L. Her, Y. H. Matsuda, K. Suga, K. Kindo, S. Takeyama, H. Berger, and H. D. Yang(2009), arXiv:0906.4856.
- ³⁸ H. Yoshida, Y. Okamoto, T. Tayama, T. Sakakibara, M. Tokunaga, A. Matsuo, Y. Narumi, K. Kindo, M. Yoshida, M. Takigawa, and Z. Hiroi, *J. Phys. Soc. Jpn.* **78**, 043704 (2009), arXiv:0902.3028.
- ³⁹ M. Yoshida, M. Takigawa, H. Yoshida, Y. Okamoto, and Z. Hiroi, *Phys. Rev. Lett.* **103**, 077207 (2009), arXiv:0906.2846.
- ⁴⁰ T. Amemiya, M. Yano, K. Morita, I. Umegaki, T. Ono, H. Tanaka, K. Fujii, and H. Uekusa(2009), arXiv:0906.1628.
- ⁴¹ T. Ono, K. Morita, M. Yano, H. Tanaka, K. Fujii, H. Uekusa, Y. Narumi, and K. Kindo, *J. Phys.: Conference Series* **145**, 012005 (2009), arXiv:0811.3291.
- ⁴² J.-H. Kim, S. Ji, S.-H. Lee, B. Lake, T. Yildirim, H. Nojiri, H. Kikuchi, K. Habicht, Y. Qiu, and K. Kiefer, *Phys. Rev. Lett.* **101**, 107201 (2008), arXiv:0806.0767.
- ⁴³ Y. Yamabe, T. Ono, T. Suto, and H. Tanaka(2006), arXiv:cond-mat/0607440.
- ⁴⁴ O. A. Petrenko, N. R. Wilson, G. Balakrishnan, D. M. Paul, and G. J. McIntyre(2010), arXiv:1005.2510.
- ⁴⁵ L. Messio, O. Cepas, and C. Lhuillier, *Phys. Rev. B* **81**, 064428 (2010), arXiv:0912.2600.
- ⁴⁶ H. Nakano and T. Sakai(2010), arXiv:1004.2528.
- ⁴⁷ E. I. Rashba, *Sov. Phys. Solid State* **2**, 1160 (1960) .
- ⁴⁸ L. Shekhtman, O. Entin-Wohlman, and A. Aharony, *Phys. Rev. Lett.* **69**, 836 (1992).
- ⁴⁹ V. Kalmeyer and R. B. Laughlin, *Phys. Rev. Lett.* **59**, 2095 (1987).
- ⁵⁰ K. Yang, L. K. Warman, and S. M. Girvin, *Phys. Rev. Lett.* **70**, 2641 (1993) .
- ⁵¹ X.-G. Wen, F. Wilczek, and A. Zee, *Phys. Rev. B* **39**, 11413 (1989).
- ⁵² F. Wang and T. Senthil, *ArXiv e-prints* (2010), arXiv:1011.3500 [cond-mat.str-el] .